Lawrence Berkeley National Laboratory
Recent Work

Title
Invariant jet mass measurements in pp collisions at s =200 GeV at RHIC

Permalink

Journal

ISSN

Authors
Abdallah, MS
Adam, J
Adamczyk, L
et al.

Publication Date

DOI

Peer reviewed

Invariant jet mass measurements in *pp* collisions at $\sqrt{s} = 200$ GeV at RHIC

M. S. Abdallah,[5] J. Adam,[6] L. Adamczyk,[2] J. R. Adams,[39] J. K. Adkins,[30] G. Agakishiev,[28] I. Aggarwal,[41]
M. M. Aggarwal,[41] Z. Ahammed,[61] I. Alekseev,[3,35] D. M. Anderson,[55] A. Aparin,[28] E. C. Aschenauer,[6] M. U. Ashraf,[11]
F. G. Atetalla,[29] A. Attri,[41] G. S. Averichev,[28] V. Bairathi,[53] W. Baker,[10] J. G. Ball Cap,[20] K. Barish,[10] A. Behera,[52]
R. Bellwied,[20] P. Bhagat,[27] A. Bhasin,[27] J. Bielcik,[14] J. Bielcikova,[38] I. G. Bordyuzhin,[3] J. D. Brandenburg,[6]
A. V. Brandin,[35] I. Bunzarov,[28] J. Butterworth,[45] X. Z. Cai,[50] H. Caines,[64] M. Calderón de la Barca Sánchez,[8] D. Cebra,[8]
I. Chakaberia,[31,6] P. Chaloupka,[14] B. K. Chan,[9] F-H. Chang,[37] Z. Chang,[6] N. Chankova-Bunzarova,[28] A. Chatterjee,[11]
S. Chattopadhyay,[61] D. Chen,[10] J. Chen,[49] J. H. Chen,[18] X. Chen,[48] Z. Chen,[49] J. Cheng,[57] M. Chevalier,[10] S. Choudhury,[18]
W. Christie,[6] X. Chu,[6] H. J. Crawford,[7] M. Csanád,[16] M. Daugherity,[1] T. G. Dedovich,[28] I. M. Deppner,[19]
A. A. Derevschikov,[43] A. Dhamija,[41] L. Di Carlo,[63] L. Didenko,[6] X. Dong,[31] J. L. Drachenberg,[1] J. C. Dunlop,[6] N. Elsey,[63]
J. Engelage,[7] G. Eppley,[45] S. Esumi,[58] O. Evdokimov,[12] A. Ewigleben,[32] O. Eyser,[6] R. Fatemi,[30] F. M. Fawzi,[5] S. Fazio,[6]
P. Federic,[38] J. Fedorisin,[28] C. J. Feng,[37] Y. Feng,[44] P. Filip,[28] E. Finch,[51] Y. Fisyak,[6] A. Francisco,[64] C. Fu,[11] L. Fulek,[2]
C. A. Gagliardi,[55] T. Galatyuk,[15] F. Geurts,[45] N. Ghimire,[54] A. Gibson,[60] K. Gopal,[23] X. Gou,[49] D. Grosnick,[60] A. Gupta,[27]
W. Guryn,[6] A. I. Hamad,[29] A. Hamed,[5] Y. Han,[45] S. Harabasz,[15] M. D. Harasty,[8] J. W. Harris,[64] H. Harrison,[30] S. He,[11]
W. He,[18] X. H. He,[26] Y. He,[49] S. Heppelmann,[8] S. Heppelmann,[42] N. Herrmann,[19] E. Hoffman,[20] L. Holub,[14] Y. Hu,[18]
H. Huang,[37] H. Z. Huang,[9] S. L. Huang,[52] T. Huang,[37] X. Huang,[57] Y. Huang,[57] T. J. Humanic,[39] D. Isenhower,[1]
W. W. Jacobs,[25] C. Jena,[23] A. Jentsch,[6] Y. Ji,[31] J. Jia,[6,52] K. Jiang,[48] X. Ju,[48] E. G. Judd,[7] S. Kabana,[53] M. L. Kabir,[10]
S. Kagamaster,[32] D. Kalinkin,[25,6] K. Kang,[57] D. Kapukchyan,[10] K. Kauder,[6] H. W. Ke,[6] D. Keane,[29] A. Kechechyan,[28]
Y. V. Khyzhniak,[35] D. P. Kikoła,[62] C. Kim,[10] B. Kimelman,[8] D. Kincses,[16] I. Kisel,[17] A. Kiselev,[6] A. G. Knospe,[32]
L. Kochenda,[35] L. K. Kosarzewski,[14] L. Kramarik,[14] P. Kravtsov,[35] L. Kumar,[41] S. Kumar,[26] R. Kunnawalkam Elayavalli,[64]
J. H. Kwasizur,[25] R. Lacey,[52] S. Lan,[11] J. M. Landgraf,[6] J. Lauret,[6] A. Lebedev,[6] R. Lednicky,[28] J. H. Lee,[6] Y. H. Leung,[31]
C. Li,[49] C. Li,[48] W. Li,[45] X. Li,[48] Y. Li,[57] X. Liang,[10] Y. Liang,[29] R. Licenik,[38] T. Lin,[55] Y. Lin,[11] M. A. Lisa,[39] F. Liu,[11]
H. Liu,[25] P. Liu,[52] T. Liu,[64] X. Liu,[39] Y. Liu,[55] Z. Liu,[48] T. Ljubicic,[6] W. J. Llope,[63] R. S. Longacre,[6] E. Loyd,[10]
N. S. Lukow,[54] X. Luo,[11] L. Ma,[18] R. Ma,[6] Y. G. Ma,[18] N. Magdy,[12] R. Majka,[64,*] D. Mallick,[36] S. Margetis,[29] C. Markert,[56]
H. S. Matis,[31] J. A. Mazer,[46] N. G. Minaev,[43] S. Mioduszewski,[55] B. Mohanty,[36] M. M. Mondal,[52] I. Mooney,[63]
D. A. Morozov,[43] A. Mukherjee,[16] M. Nagy,[16] J. D. Nam,[54] Md. Nasim,[22] K. Nayak,[11] D. Neff,[9] J. M. Nelson,[7]
D. B. Nemes,[64] M. Nie,[49] G. Nigmatkulov,[35] T. Niida,[58] R. Nishitani,[58] L. V. Nogach,[43] T. Nonaka,[58] A. S. Nunes,[6]
G. Odyniec,[31] A. Ogawa,[6] S. Oh,[31] V. A. Okorokov,[35] B. S. Page,[6] R. Pak,[6] A. Pandav,[36] A. K. Pandey,[58] Y. Panebratsev,[28]
P. Parfenov,[35] B. Pawlik,[40] D. Pawlowska,[62] H. Pei,[11] C. Perkins,[7] L. Pinsky,[20] R. L. Pintér,[16] J. Pluta,[62] B. R. Pokhrel,[54]
G. Ponimatkin,[38] J. Porter,[31] M. Posik,[54] V. Prozorova,[14] N. K. Pruthi,[41] M. Przybycien,[2] J. Putschke,[63] H. Qiu,[26]
A. Quintero,[54] C. Racz,[10] S. K. Radhakrishnan,[29] N. Raha,[63] R. L. Ray,[56] R. Reed,[32] H. G. Ritter,[31] M. Robotkova,[38]
O. V. Rogachevskiy,[28] J. L. Romero,[8] L. Ruan,[6] J. Rusnak,[38] N. R. Sahoo,[49] H. Sako,[58] S. Salur,[46] J. Sandweiss,[64,*]
S. Sato,[58] W. B. Schmidke,[6] N. Schmitz,[33] B. R. Schweid,[52] F. Seck,[15] J. Seger,[13] M. Sergeeva,[9] R. Seto,[10] P. Seyboth,[33]
N. Shah,[24] E. Shahaliev,[28] P. V. Shanmuganathan,[6] M. Shao,[48] T. Shao,[50] A. I. Sheikh,[29] D. Shen,[50] S. S. Shi,[11] Y. Shi,[49]
Q. Y. Shou,[18] E. P. Sichtermann,[31] R. Sikora,[2] M. Simko,[38] J. Singh,[41] S. Singha,[26] M. J. Skoby,[44] N. Smirnov,[64]
Y. Söhngen,[19] W. Solyst,[25] P. Sorensen,[6] H. M. Spinka,[4,*] B. Srivastava,[44] T. D. S. Stanislaus,[60] M. Stefaniak,[62]
D. J. Stewart,[64] M. Strikhanov,[35] B. Stringfellow,[44] A. A. P. Suaide,[47] M. Sumbera,[38] B. Summa,[42] X. M. Sun,[11] X. Sun,[12]
Y. Sun,[48] Y. Sun,[21] B. Surrow,[54] D. N. Svirida,[3] Z. W. Sweger,[8] P. Szymanski,[62] A. H. Tang,[6] Z. Tang,[48] A. Taranenko,[35]
T. Tarnowsky,[34] J. H. Thomas,[31] A. R. Timmins,[20] D. Tlusty,[13] T. Todoroki,[58] M. Tokarev,[28] C. A. Tomkiel,[32]
S. Trentalange,[9] R. E. Tribble,[55] P. Tribedy,[6] S. K. Tripathy,[16] T. Truhlar,[14] B. A. Trzeciak,[14] O. D. Tsai,[9] Z. Tu,[6] T. Ullrich,[6]
D. G. Underwood,[4] I. Upsal,[49,6] G. Van Buren,[6] J. Vanek,[38] A. N. Vasiliev,[43] I. Vassiliev,[17] V. Verkest,[63] F. Videbaek,[6]
S. Vokal,[28] S. A. Voloshin,[63] F. Wang,[44] G. Wang,[9] J. S. Wang,[21] P. Wang,[48] Y. Wang,[11] Y. Wang,[57] Z. Wang,[49] J. C. Webb,[6]
P. C. Weidenkaff,[19] L. Wen,[9] G. D. Westfall,[34] H. Wieman,[31] S. W. Wissink,[25] R. Witt,[59] J. Wu,[26] Y. Wu,[10] B. Xi,[50]
Z. G. Xiao,[57] G. Xie,[31] W. Xie,[44] H. Xu,[21] N. Xu,[31] Q. H. Xu,[49] Y. Xu,[49] Z. Xu,[6] Z. Xu,[9] C. Yang,[49] Q. Yang,[49] Y. Yang,[37]
Z. Ye,[45] Z. Ye,[12] L. Yi,[49] K. Yip,[6] Y. Yu,[49] H. Zbroszczyk,[62] W. Zha,[48] C. Zhang,[52] D. Zhang,[11] S. Zhang,[12] S. Zhang,[18]
X. P. Zhang,[57] Y. Zhang,[26] Y. Zhang,[48] Y. Zhang,[11] Z. J. Zhang,[37] Z. Zhang,[6] Z. Zhang,[12] J. Zhao,[44] C. Zhou,[18] X. Zhu,[57]
Z. Zhu,[49] M. Zurek,[31] and M. Zyzak[17]

(STAR Collaboration)

[1]*Abilene Christian University, Abilene, Texas 79699*
[2]*AGH University of Science and Technology, FPACS, Cracow 30-059, Poland*

[3]*Alikhanov Institute for Theoretical and Experimental Physics NRC "Kurchatov Institute",*
Moscow 117218, Russia
[4]*Argonne National Laboratory, Argonne, Illinois 60439*
[5]*American University of Cairo, New Cairo 11835, New Cairo, Egypt*
[6]*Brookhaven National Laboratory, Upton, New York 11973*
[7]*University of California, Berkeley, California 94720*
[8]*University of California, Davis, California 95616*
[9]*University of California, Los Angeles, California 90095*
[10]*University of California, Riverside, California 92521*
[11]*Central China Normal University, Wuhan, Hubei 430079*
[12]*University of Illinois at Chicago, Chicago, Illinois 60607*
[13]*Creighton University, Omaha, Nebraska 68178*
[14]*Czech Technical University in Prague, FNSPE, Prague 115 19, Czech Republic*
[15]*Technische Universität Darmstadt, Darmstadt 64289, Germany*
[16]*ELTE Eötvös Loránd University, Budapest H-1117, Hungary*
[17]*Frankfurt Institute for Advanced Studies FIAS, Frankfurt 60438, Germany*
[18]*Fudan University, Shanghai 200433*
[19]*University of Heidelberg, Heidelberg 69120, Germany*
[20]*University of Houston, Houston, Texas 77204*
[21]*Huzhou University, Huzhou, Zhejiang 313000*
[22]*Indian Institute of Science Education and Research (IISER), Berhampur 760010, India*
[23]*Indian Institute of Science Education and Research (IISER) Tirupati, Tirupati 517507, India*
[24]*Indian Institute Technology, Patna, Bihar 801106, India*
[25]*Indiana University, Bloomington, Indiana 47408*
[26]*Institute of Modern Physics, Chinese Academy of Sciences, Lanzhou, Gansu 730000*
[27]*University of Jammu, Jammu 180001, India*
[28]*Joint Institute for Nuclear Research, Dubna 141 980, Russia*
[29]*Kent State University, Kent, Ohio 44242*
[30]*University of Kentucky, Lexington, Kentucky 40506-0055*
[31]*Lawrence Berkeley National Laboratory, Berkeley, California 94720*
[32]*Lehigh University, Bethlehem, Pennsylvania 18015*
[33]*Max-Planck-Institut für Physik, Munich 80805, Germany*
[34]*Michigan State University, East Lansing, Michigan 48824*
[35]*National Research Nuclear University MEPhI, Moscow 115409, Russia*
[36]*National Institute of Science Education and Research, HBNI, Jatni 752050, India*
[37]*National Cheng Kung University, Tainan 70101*
[38]*Nuclear Physics Institute of the CAS, Rez 250 68, Czech Republic*
[39]*Ohio State University, Columbus, Ohio 43210*
[40]*Institute of Nuclear Physics PAN, Cracow 31-342, Poland*
[41]*Panjab University, Chandigarh 160014, India*
[42]*Pennsylvania State University, University Park, Pennsylvania 16802*
[43]*NRC "Kurchatov Institute," Institute of High Energy Physics, Protvino 142281, Russia*
[44]*Purdue University, West Lafayette, Indiana 47907*
[45]*Rice University, Houston, Texas 77251*
[46]*Rutgers University, Piscataway, New Jersey 08854*
[47]*Universidade de São Paulo, São Paulo 05314-970, Brazil*
[48]*University of Science and Technology of China, Hefei, Anhui 230026*
[49]*Shandong University, Qingdao, Shandong 266237*
[50]*Shanghai Institute of Applied Physics, Chinese Academy of Sciences, Shanghai 201800*
[51]*Southern Connecticut State University, New Haven, Connecticut 06515*
[52]*State University of New York, Stony Brook, New York 11794*
[53]*Instituto de Alta Investigación, Universidad de Tarapacá, Arica 1000000, Chile*
[54]*Temple University, Philadelphia, Pennsylvania 19122*
[55]*Texas A&M University, College Station, Texas 77843*
[56]*University of Texas, Austin, Texas 78712*
[57]*Tsinghua University, Beijing 100084*
[58]*University of Tsukuba, Tsukuba, Ibaraki 305-8571, Japan*
[59]*United States Naval Academy, Annapolis, Maryland 21402*
[60]*Valparaiso University, Valparaiso, Indiana 46383*
[61]*Variable Energy Cyclotron Centre, Kolkata 700064, India*

[62]*Warsaw University of Technology, Warsaw 00-661, Poland*
[63]*Wayne State University, Detroit, Michigan 48201*
[64]*Yale University, New Haven, Connecticut 06520*

We present the first inclusive measurements of the invariant and SOFTDROP jet mass in proton-proton collisions at $\sqrt{s} = 200$ GeV at STAR. The measurements are fully corrected for detector effects, and reported differentially in both the jet transverse momentum and jet radius parameter. We compare the measurements to established leading-order Monte Carlo event generators and find that STAR-tuned PYTHIA-6 reproduces the data, while LHC tunes of PYTHIA-8 and HERWIG-7 do not agree with the data, providing further constraints on parameter tuning. Finally, we observe that SOFTDROP grooming, for which the contribution of wide-angle nonperturbative radiation is suppressed, shifts the jet mass distributions into closer agreement with the partonic jet mass as determined by both PYTHIA-8 and a next-to-leading-logarithmic accuracy perturbative QCD calculation. These measurements complement recent LHC measurements in a different kinematic region, as well as establish a baseline for future jet mass measurements in heavy-ion collisions at RHIC.

I. INTRODUCTION

A hard scattered parton will typically be highly virtual, and therefore will quickly radiate a gluon [1]. The cascade of further radiation and splitting is called a parton shower, which is described by the coupled differential Dokshitzer-Gribov-Lipatov-Altarelli-Parisi equations [2–4]. Once the partons' virtuality reach the nonperturbative (NP) regime, they hadronize. In order to access the initial hard-scattered parton and its evolution, the final-state particles are clustered into collective objects called jets, using algorithms defined identically in theory and experiment and robust to both arbitrarily soft and collinear radiation [5]. Jets have been used, e.g., to refine the strong coupling [6, Sec. 9.4.5], to search for new physics [7], and to improve knowledge of the parton distribution functions [8]. Measurements of jet substructure specifically test fundamental QCD via final state radiation patterns and are important in a heavy-ion context due to, e.g., possible coherent energy loss of hard scattered partons in the QCD medium [9]. In this paper, we present the measurement of a jet substructure observable called the jet mass, M, defined as the magnitude of the four-momentum sum of the jet constituents, $M = |\sum_{i \in \text{jet}} p_i| = \sqrt{E^2 - \boldsymbol{p}^2}$, where E and $\boldsymbol{p}$ are the energy and three-momentum of the jet, respectively (see [10–17] for previous measurements at the LHC and the Tevatron). The influence of the initial hard scattering, fragmentation, and hadronization on the resulting jet

angular and momentum scales implies that the jet mass is sensitive to the details of these processes. The mass of jets arising from heavy quarks is also sensitive to the initiating quark's mass (see Ref. [15] for an extraction of the top quark mass from top quark jets) although in the kinematic regime of this paper, light quark jets are dominant [18], and access instead the initiating parton's virtuality. We can use the jet mass distributions to test the applicability of perturbative QCD (PQCD) calculations at low jet energies and also to tune parton shower parameters in Monte Carlo (MC) event generators such as PYTHIA and HERWIG [19–21] for better prediction power across varying center-of-mass energies.

Jet mass is sensitive to both perturbative and nonperturbative physics. At the Relativistic Heavy Ion Collider (RHIC), the lower center-of-mass energy, $\sqrt{s}$, compared to the Large Hadron Collider (LHC), reduces the importance of higher-order (N^nLO) effects, while the lower jet transverse momentum, $p_{\text{T,jet}}$, increases the sensitivity to the underlying event and hadronization [22]. However, one may reduce contributions of NP physics such as the underlying event and hadronization in a Sudakov-safe way [23] with the SOFTDROP grooming algorithm [24], which is described in more detail in Sec. II. Therefore, a groomed jet mass measurement, i.e., a jet mass measurement on a population of jets to which the SOFTDROP grooming algorithm has been applied, allows a more direct comparison with analytic calculations [25] at varying orders. We would also expect that the Sudakov peak—the result of a small probability of low and high mass jets due to suppression of perfectly collinear gluon radiation after resummation and hard or wide-angle radiation, respectively—shifts to lower jet mass after SOFTDROP grooming due to the removal of wide-angle radiation [26]. Additionally, a comparison of groomed jet mass to

---

*Deceased.

ungroomed jet mass differentially in $p_{\mathrm{T,jet}}$, and the jet radius parameter, R, can be utilized to assess experimentally the phase space for which the magnitude of NP effects is significant.

The jet mass is also a useful quantity in heavy-ion collisions (see [17] for a previous measurement at the LHC), in which any hard scatters occur before the hot, dense, colored QCD medium is formed. The partons, which also carry color charge, then interact with the medium which may temporarily increase the virtuality of the jets causing an increase in gluon radiation (increasing the jet mass), while on the whole, virtuality will decrease more quickly in the medium (decreasing the jet mass) [17]. Therefore, this measurement will serve as a vacuum baseline for a future measurement in heavy-ion collisions, in which medium modification of the jet mass in a hot, dense nuclear environment may be observed [27].

In pp collisions, there have been several recent jet mass measurements [10–16] (almost exclusively at the LHC) and calculations [28–35] (at LHC kinematics) demonstrating that LHC-tuned MC simulations and calculations are able to describe the data at LHC energies. This paper presents the first fully corrected inclusive jet mass measurement at RHIC energies.

In this paper, we present the ungroomed and groomed jet mass differentially in both $p_{\mathrm{T,jet}}$ and R, where jets are reconstructed with the FASTJET anti-k_{T} algorithm [5,36]. We compare to three MC simulations in this analysis: PYTHIA-6, HERWIG-7, and PYTHIA-8. We also show a PYTHIA-8 parton-level simulation and a PQCD calculation at next-to-leading-logarithmic (NLL) accuracy to emphasize the suppression of NP effects by grooming.

II. EXPERIMENTAL SETUP

The data used for this analysis were collected by the Solenoidal Tracker at RHIC (STAR) detector in pp collisions at $\sqrt{s} = 200$ GeV in 2012. Charged tracks are reconstructed via the Time Projection Chamber (TPC) [37], and the surrounding Barrel Electromagnetic Calorimeter (BEMC) [38] measures electromagnetic energy deposits in its 4800 towers each covering 0.05×0.05 in pseudorapidity (η) and azimuth (ϕ). These detectors have full azimuthal coverage and $|\eta| < 1$. In a procedure called hadronic correction, the tower energy is corrected for energy from tracks measured in the TPC which match to the tower, to avoid double-counting. Any negative corrected tower energies are set to zero. This procedure is optimal with respect to the result on the jet momentum resolution and neutral energy fraction [39]. The BEMC is additionally used online as an event trigger that requires a total analogue-to-digital converter value above a certain threshold, corresponding to $\sum E_{\mathrm{T,tower}} > 7.3$ GeV, in one of 18 partially overlapping 1.0×1.0 $\eta \times \phi$ groupings of towers called Jet Patches [40].

For the analysis we impose certain quality requirements on the tracks and towers, e.g., $0.2 < p_{\mathrm{T}} < 30$ GeV/c, $0.2 < E_{\mathrm{T}} < 30$ GeV, and $|\eta| < 1$, as well as standard overall event quality assurance cuts [40]. Namely, we require the z component of the primary vertex location to be within 30 cm of the center of the detector, and due to worsening momentum resolution for high-p_{T} tracks, we reject events containing tracks with $p_{\mathrm{T}} > 30$ GeV/c or towers with $E_{\mathrm{T}} > 30$ GeV. Although three of the components of the particle or tower four-vector are specified, the mass is unknown, so we choose a mass assignment. This analysis does not attempt any particle identification, so at detector-level (i.e., data and simulation in which particles traverse detector material), the pion mass is assumed for charged tracks, and tower energy deposits are assumed massless; at particle-level (i.e., vacuum simulation), the particle PDG mass [6] is assigned (as in Ref. [17]). The effect of the difference between detector level and particle level caused by this choice of mass assignments is folded into the detector response, and is corrected via unfolding so that the reported particle-level data is comparable to MC simulations and analytic calculations using the hadrons' PDG mass.

We cluster accepted tracks and towers into jets using the anti-k_{T} sequential recombination algorithm with the E scheme in the FASTJET framework. This algorithm defines distance metrics

$$d_{ij} = \min\left(p_{\mathrm{T},i}^{-2}, p_{\mathrm{T},j}^{-2}\right) \frac{\Delta_{ij}^2}{R^2}$$

and $d_{iB} = p_{\mathrm{T},i}^{-2}$, where $\Delta_{ij}^2 = (y_i - y_j)^2 + (\phi_i - \phi_j)^2$, and y_i is the rapidity of object i. It then finds the smallest distance among objects; it recombines i and j if d_{ij} is the smallest distance, or removes i from consideration and considers it a jet if d_{iB} is the smallest distance. This is repeated until only jets remain. In the analysis, jets are selected to be contained within the experimental fiducial volume of the TPC and BEMC ($|\eta_{\mathrm{jet}}| < 1 - R$, where η_{jet} is the pseudorapidity of the jet axis). In addition, we consider only jets with less than 90% of their energy from the BEMC to reduce the contribution of beam background [40]. After all event, track, tower, and jet cuts, the remaining jet population is considered for the ungroomed mass analysis.

The SOFTDROP declustering algorithm is then applied to these jets to obtain a population of groomed jets. That is, jets are reclustered in an angular-ordered tree (with the Cambridge-Aachen algorithm [41,42]), and starting with the outermost constituent pairs (denoted with the subscripts 1 and 2), those failing the condition

$$\frac{\min\left(p_{\mathrm{T},1}, p_{\mathrm{T},2}\right)}{p_{\mathrm{T},1} + p_{\mathrm{T},2}} > z_{\mathrm{cut}} \left(\frac{\Delta_{12}}{R}\right)^{\beta}$$

have the softer constituent removed; the procedure is iterated until either a pair passes the condition ("grooming

mode") or the jet can no longer be declustered ("tagging mode"). Here, β controls the extent to which wide-angle constituents are removed, and z_{cut} is the momentum sharing fraction threshold for the pair. For example, $z_{cut} = 0.2$, $\beta = 0$ denotes that the softer constituent must carry 20% of the overall momentum of the pair, with no angular consideration. We apply the SOFTDROP grooming procedure in tagging mode with $z_{cut} = 0.1$ and $\beta = 0$ to these ungroomed jets, to obtain the population of jets to be considered for the groomed mass analysis. This canonical choice of parameters simplifies calculations [24]. It was also shown, ibid., in a PYTHIA-8 study at LHC energies that an observable similar to jet mass has very little contribution from hadronization corrections or underlying event, after grooming with the parameters used in this analysis. This provides evidence for the suppression of NP effects by the SOFTDROP declustering procedure. In this paper, observables on the set of groomed jets are subscripted with a "g," and are shown for ranges of the corresponding ungroomed $p_{T,jet}$, to allow a direct comparison between jet mass and groomed jet mass.

III. CORRECTION FOR DETECTOR EFFECTS

To correct for detector effects, we use a two-dimensional Bayesian unfolding procedure [43]; with this we obtain the physical distributions ("causes") most likely to have lead to the observed data ("effects"), using Bayesian inference. We construct two detector response matrices, one for $p_{T,jet}$ and M, and one for $p_{T,jet}$[1] and M_g, and unfold (in M and M_g separately) the uncorrected data to particle-level via the ROOUNFOLD package [44] with a regularization parameter of 4. This parameter corresponds to the number of iterations of the Bayesian inference procedure: each subsequent iteration uses as a prior the posterior from the previous iteration, so that larger numbers of iterations yield less reliance on the initial prior distribution given in this case by Monte Carlo simulations. However, beyond some number of iterations, the statistical uncertainties grow rapidly, hence the choice of 4.

A visualization of a subset of the four-dimensional response matrix is shown in Fig. 1, with particle-level (detector-level) jet mass denoted $M_{part(det)}$. To construct the matrix, we begin with a sample of pp events at $\sqrt{s} = 200$ GeV generated by the PYTHIA-6.428 event generator with CTEQ6L1 parton distribution functions [45] and the PERUGIA 2012 tune, further tuned to STAR data (see Refs. [18,40] for details). These particle-level events are then passed to the GEANT-3 [46] STAR detector simulation to obtain the detector hits, and are combined with zero-bias (randomly triggered) data from the same pp run period. Detector-level events, from the GEANT simulation, are

---

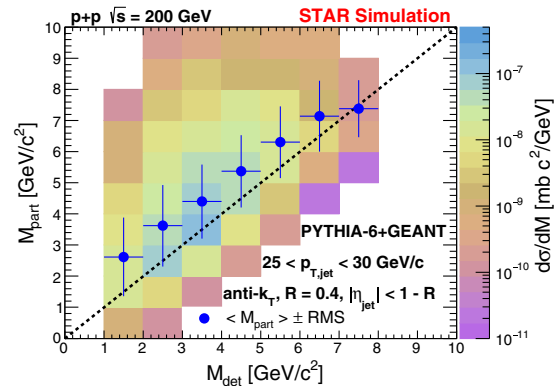[1]Note that throughout, M_g is shown as a function of p_T of the ungroomed (rather than groomed) jet.

FIG. 1. Correlation between simulated jet mass at particle level (given by PYTHIA-6) and detector level (given by PYTHIA-6+GEANT) for a single $p_{T,jet}$ selection at both particle and detector levels ($25 < p_{T,jet} < 30$ GeV/c) and jet radius parameter $R = 0.4$. The mean particle-level mass for a particular detector-level mass selection is given by the blue circles, with horizontal bars spanning the detector-level jet mass bin width and vertical bars denoting the particle-level jet mass rms for that selection of M_{det}.

treated exactly like events in the data as described in Sec. II. The (groomed) jet mass from PYTHIA-6 and PYTHIA-6+GEANT is shown on the (right) left in Fig. 2 with a comparison to the uncorrected data, for $R = 0.4$ jets with $20 < p_{T,jet} < 25$ GeV/c. We observe good agreement between the uncorrected data and detector simulation, as shown in the ratio panel. Similar agreement is found in all three of the $p_{T,jet}$ selections reported in this paper. Note that the ungroomed detector-level jet mass is required to be greater than 1 GeV/c^2 to improve the performance of the unfolding procedure. The groomed mass has no such restriction.

To compare the particle- and detector-level jets on a jet-by-jet basis, we match geometrically by requiring potential matches to pass the criterion,

$$\sqrt{(\Delta\eta)^2 + (\Delta\phi)^2} < R,$$

where $\Delta\eta$ ($\Delta\phi$) denotes the difference between the particle- and detector-level jet axes in η (ϕ). A match is a jet pair that satisfies the above criterion and falls in the jet momentum and jet mass ranges of the response matrix (namely at particle level, $p_{T,jet} \in (5, 80)$ GeV/c, and at detector level $p_{T,jet} \in (15, 60)$ GeV/c and $M > 1$ GeV/c^2). The detector performance is quantified by a ratio, r, of detector-level to particle-level mass on a jet-by-jet basis for the matched pairs. This is shown in Fig. 3 for jet mass on the left and groomed mass on the right, for $R = 0.4$ jets with $20 < p_{T,jet} < 25$ GeV/c as black circles, $25 < p_{T,jet} < 30$ GeV/c as red squares, and $30 < p_{T,jet} < 40$ GeV/c as blue crosses. Tracking inefficiency of the detector reduces the jet mass, shifting the peak of the distribution to the left of unity. We observe that the
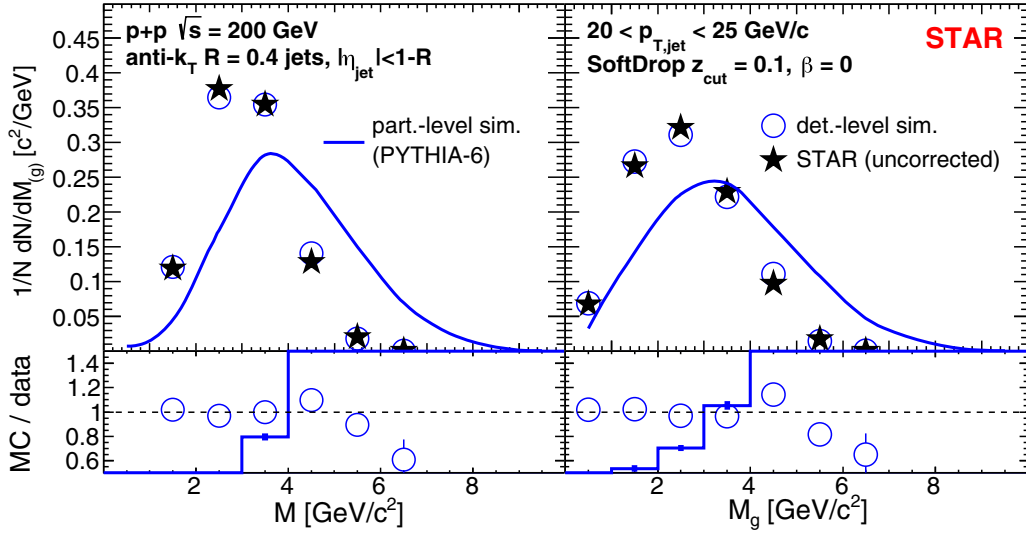
FIG. 2. Comparison of STAR data (full star markers), particle-level simulation given by PYTHIA-6 (PERUGIA 2012 STAR Tune, solid blue line), and detector-level simulation given by PYTHIA-6+GEANT (open blue circles) for jet mass, M (left) and groomed jet mass, M_g (right) for a single $p_{T,jet}$ selection ($20 < p_{T,jet} < 25$ GeV/c) and $R = 0.4$. Data are uncorrected for detector effects. Statistical uncertainties are smaller than the size of the markers. We quantitatively compare via ratio in the lower panels to the particle- and detector-level simulations.
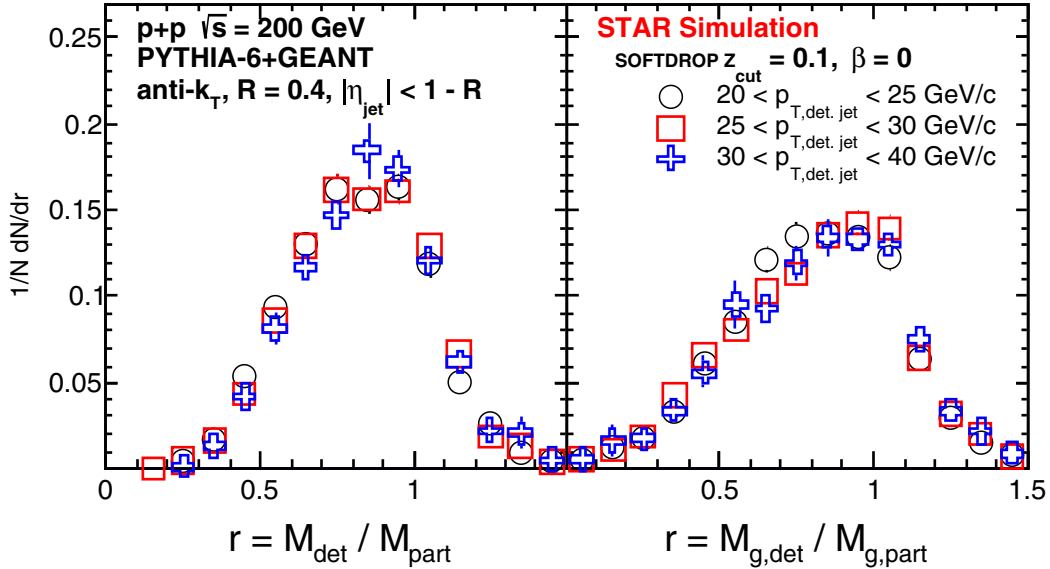
FIG. 3. Ratio of simulated detector-level to particle-level jet mass (ungroomed and groomed, respectively) for three selections of detector-level $p_{T,jet}$ (with no selection on the corresponding particle-level $p_{T,jet}$), for $R = 0.4$ particle-level jets from PYTHIA-6 matched event by event to detector-level jets from PYTHIA-6+GEANT. Most statistical uncertainties—denoted by vertical bars—are smaller than the size of the markers.

resolution (the width of the distribution) is independent of $p_{T,jet}$, which is beneficial for numerical stability in the unfolding. There are relatively more groomed jets than ungroomed jets with low r (say, $r < 0.5$), due to the lack of a minimum detector-level M_g requirement mentioned

above. We use the resolution to determine the appropriate jet mass bin width (1 GeV/c^2) used in the unfolding procedure, while the $p_{T,jet}$ bin width (5 GeV/c) is the same as what was used in Ref. [40]. The highest $p_{T,jet}$ selection for which we show the jet mass ($30 < p_{T,jet} < 40$ GeV/c) is wider, as in

TABLE I. Systematic uncertainties for an example jet population with $25 < p_{\rm T,jet} < 30$ GeV/c and, from the top to the bottom row, $1 < M_{\rm (g)} < 2$, $4 < M_{\rm (g)} < 5$, and $7 < M_{\rm (g)} < 8$ GeV/c^2. The total systematic uncertainties are obtained by adding the sources in the four preceding columns in quadrature. Upper: ungroomed jet mass. Lower: groomed jet mass.

Source / Range in M	Hadronic correction	Tower gain	Tracking efficiency	Unfolding procedure	Total systematics
$(1, 2)$ GeV/c^2	1.3%	0.9%	13.0%	12.2%	17.9%
$(4, 5)$ GeV/c^2	0.1%	0.6%	0.4%	4.1%	4.1%
$(7, 8)$ GeV/c^2	3.6%	0.4%	6.9%	22.9%	24.1%

Source / Range in $M_{\rm g}$	Hadronic correction	Tower gain	Tracking efficiency	Unfolding procedure	Total systematics
$(1, 2)$ GeV/c^2	2.6%	0.7%	6.8%	9.1%	11.7%
$(4, 5)$ GeV/c^2	1.0%	0.8%	1.5%	3.4%	4.0%
$(7, 8)$ GeV/c^2	1.1%	0.2%	8.0%	28.3%	29.4%

that paper, in order to improve the low statistics at higher $p_{\rm T,jet}$ due to the steeply falling $p_{\rm T,jet}$ spectrum at RHIC.

IV. SYSTEMATIC UNCERTAINTIES

There are four sources of systematic uncertainty involved in the jet mass analysis. Two detector uncertainties were considered: uncertainty on the tower gain calibration (3.8%) and on the tracking efficiency (4%) [18]. Two procedural uncertainties were considered as well. The first, the hadronic correction, is varied from the nominal subtraction of 100% of a track's p_T from the matched tower, to 50% which is between the average charged hadron energy deposition in the BEMC and the nominal over-subtraction of 100%. In addition, there is uncertainty arising from the unfolding procedure [40].

The unfolding procedure outlined in Sec. III is a dominant source of systematic uncertainties. We vary the regularization parameter from the nominal value of 4 down to 2 (the minimum for an iterative Bayesian approach) and up to 6 (above which the influence of statistical fluctuations is large). We also vary the shape of the particle-level $p_{\rm T,jet}$ spectrum prior distribution given by PYTHIA-6 as well as the detector-level $p_{\rm T,jet}$ spectrum given by PYTHIA-6+GEANT. Similarly, we vary the shape of the particle-level mass spectrum prior distribution given by PYTHIA-6, which is adjusted by the ratios of PYTHIA-6 to PYTHIA-8 and to HERWIG-7. The two particle-level Bayesian prior smearings contribute roughly equally to the relative systematic uncertainty, while the detector-level $p_{\rm T,jet}$ spectrum variation is subdominant. The maximum envelope of these variations is taken as the unfolding uncertainty.

The individual sources and total systematic uncertainties (the quadrature sum of individual contributions) are shown in Table I for representative $p_{\rm T,jet}$ and $M_{\rm (g)}$ selections. Relative uncertainty values in Table I were obtained by propagating each variation through the unfolding procedure, and dividing the resulting fully corrected mass by the nominal result.

V. RESULTS

The fully corrected jet mass and groomed jet mass distributions are shown in Fig. 4 for $R = 0.4$ jets with $20 < p_{\rm T,jet} < 25$ GeV/c in the left panel, $25 < p_{\rm T,jet} < 30$ GeV/c in the middle panel, and $30 < p_{\rm T,jet} < 40$ GeV/c in the right panel. As $p_{\rm T,jet}$ increases, we observe an increase in the mean mass, $\langle M \rangle$, and groomed mass, $\langle M_{\rm g} \rangle$, as well as a broadening of the distribution: jet mass and groomed jet mass mean (rms) increase by $25.5\% \pm 0.2\%({\rm stat}) \pm 2.0\%({\rm syst})$ $(18.1\% \pm 0.4\% \pm 4.1\%)$ and $15.5\% \pm 0.3\% \pm 2.4\%$ $(23.2\% \pm 0.4\% \pm 3.6\%)$, respectively, from lowest to highest $p_{\rm T,jet}$. This is due to the increase in the available phase space for radiation with higher jet momentum, as expected from PQCD, although the effect is slightly mitigated by the relative increase, as $p_{\rm T,jet}$ increases, in the number of quark-initiated jets, which have lower $\langle M \rangle$ than gluon-initiated jets [47].

We compare our fully corrected results with leading-order MC event generators PYTHIA-8 (including a curve with hadronization turned off, which we denote "parton jets"), HERWIG-7, and PYTHIA-6. The latter uses the PERUGIA 2012 tune [48] with additional tuning to the RHIC environment [18]. The former two use tunes developed for LHC kinematics—in PYTHIA-8 the MONASH 2013 tune [49], and in HERWIG-7 the EE4C underlying event tune [50]. Relevant model differences between PYTHIA and HERWIG for a jet substructure analysis lie in the shower and hadronization mechanisms, where PYTHIA uses a p_T-ordered shower and string fragmentation, while HERWIG uses an angular-ordered shower and cluster hadronization.

We note that PYTHIA-6 describes the data well, within systematic uncertainties, whereas the HERWIG-7 and PYTHIA-8 prefer lower and higher mass jets, respectively, as observed in the slope of the ratio of MC simulations to data. The behavior of HERWIG-7 and PYTHIA-8 is similar to that of HERWIG and PYTHIA (albeit different versions and tunes) in the LHC measurement of Ref. [10], although with HERWIG preferring larger mass jets and PYTHIA preferring slightly smaller mass jets than data. We also observe from
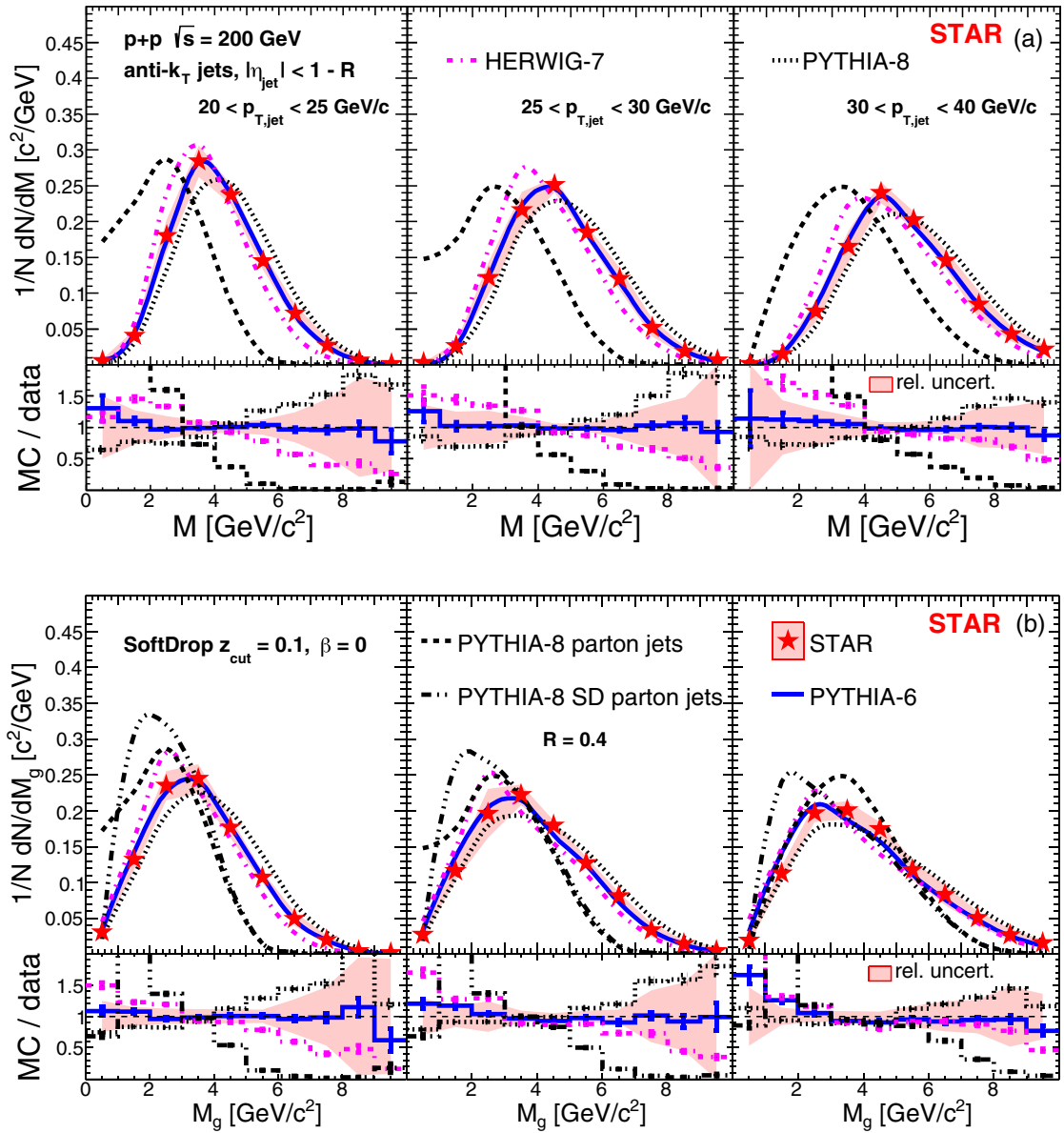
FIG. 4.   Distributions of (a) M and (b) M_g for $R = 0.4$ anti-k_T jets in pp collisions at $\sqrt{s} = 200$ GeV. From left to right, the $p_{T,\text{jet}}$ increases from $20 < p_{T,\text{jet}} < 25$ GeV/c to $30 < p_{T,\text{jet}} < 40$ GeV/c. The fully corrected data (with accompanying red shaded band denoting systematic uncertainties) are shown as solid red star markers. We quantitatively compare via ratio ("MC/data") to PYTHIA-6 (PERUGIA 2012 STAR Tune, solid blue line), PYTHIA-8 (MONASH 2013 Tune, dotted black line), and HERWIG-7 (EE4C Tune, dot-dashed magenta line) in the lower part of each panel, along with a total relative systematic uncertainty ("rel. uncert.") on the data (corresponding to the absolute systematic uncertainty given by the shaded red band in the upper part of the panels). PYTHIA-8 with hadronization turned off is also shown as "PYTHIA-8 parton jets" (dashed black line). Statistical uncertainties are smaller than the size of the markers. In (b), we additionally compare to PYTHIA-8 parton-level M (dashed black line) and M_g (dot-dashed black line, denoted "SD" in the legend for SOFTDROP groomed jets). The groomed parton-level curve is sometimes higher than its ungroomed counterpart because we drop jets with $z_g < 0.1$, which are also often low mass jets.

the comparison of the parton-level to hadron-level curves from PYTHIA-8 that hadronization increases the jet mass. In addition to the scan over $p_{T,\text{jet}}$, we show in Fig. 5 the jet mass and groomed jet mass distributions for jet radius

$R = 0.2$, 0.4, and 0.6, for a fixed $p_{T,\text{jet}}$ from 30 to 40 GeV/c. We observe that the mass increases with increasing R, which is expected as the jet will encompass more wide-angle NP physics and will more often be a
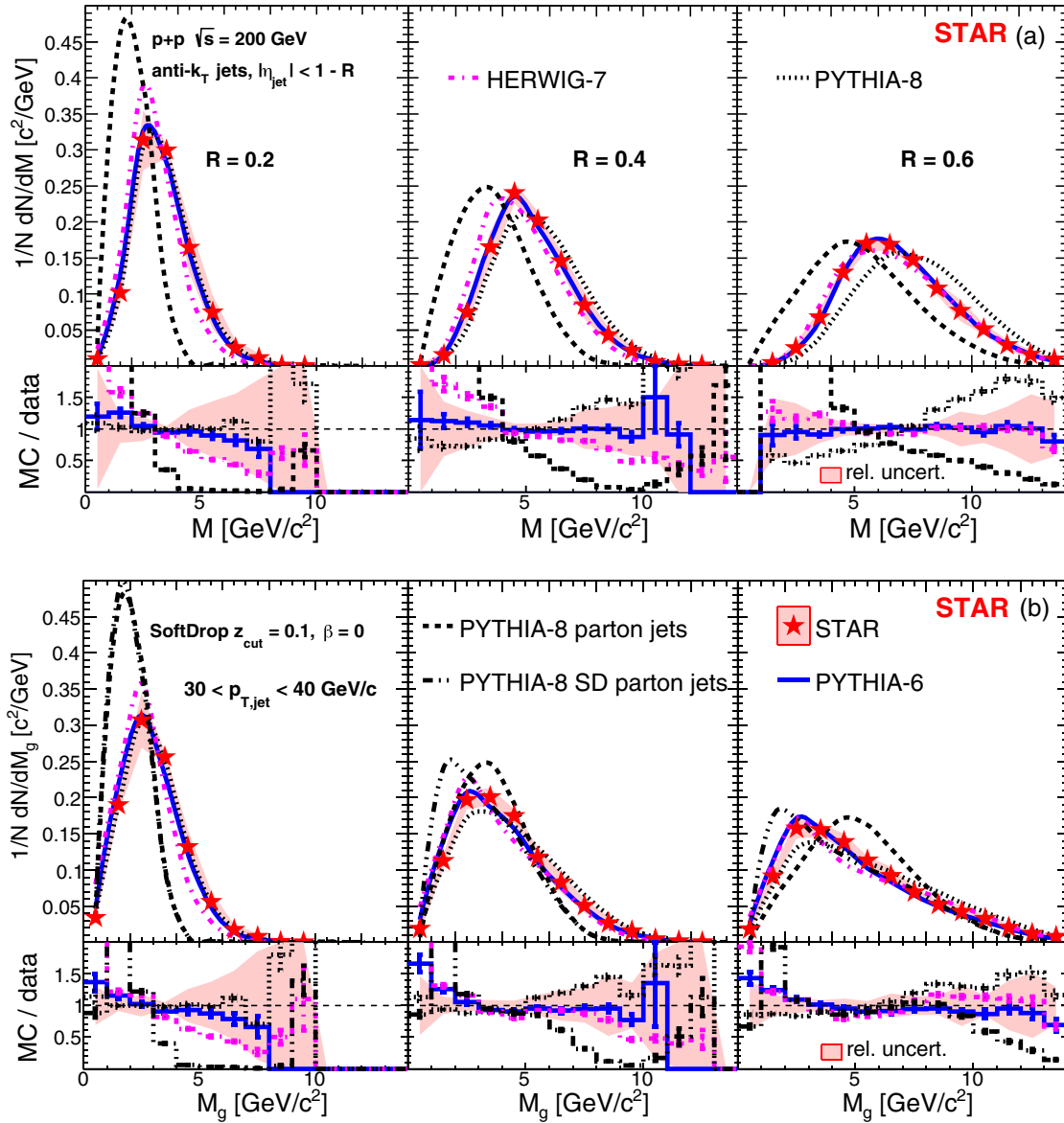
FIG. 5. Distributions of (a) M and (b) M_g for anti-k_T jets in pp collisions at $\sqrt{s} = 200$ GeV for a single $p_{T,jet}$ selection ($30 < p_{T,jet} < 40$ GeV/c) and varying jet radii (from left to right, $R = 0.2, 0.4, 0.6$). The style of the curves is the same as in Fig. 4. Statistical uncertainties are smaller than the size of the markers. In (b), we additionally compare to groomed PYTHIA-8 parton level (dot-dashed black line, denoted "SD" in the legend for SOFTDROP groomed jets) and ungroomed PYTHIA-8 parton level (dashed black line) to demonstrate that grooming removes NP physics such as hadronization.

gluon-initiated jet which has higher mass on average than a quark-initiated jet.

As for the groomed mass, it exhibits similar trends of increasing mass with increasing $p_{T,jet}$ and R. We note, however, that the position of the Sudakov peak is shifted up to $55\% \pm 22\%$(stat) lower, for the largest jet radius and $p_{T,jet}$ selection, for the groomed mass compared to the ungroomed mass distributions. This implies that jet constituents arising from wide-angle radiation are indeed

suppressed. We also observe that the grooming procedure results in a groomed mass that is closer to the ungroomed parton-level curves, signaling that NP effects such as hadronization have been reduced. Both of these effects are more significant for $R = 0.6$ jets. Finally, we note that for ungroomed mass, PYTHIA-6 is consistent with the data in all cases, while for groomed mass, PYTHIA-6 slightly underpredicts data for all jet radii shown. HERWIG-7 and PYTHIA-8 prefer lower and higher mass jets, respectively, in
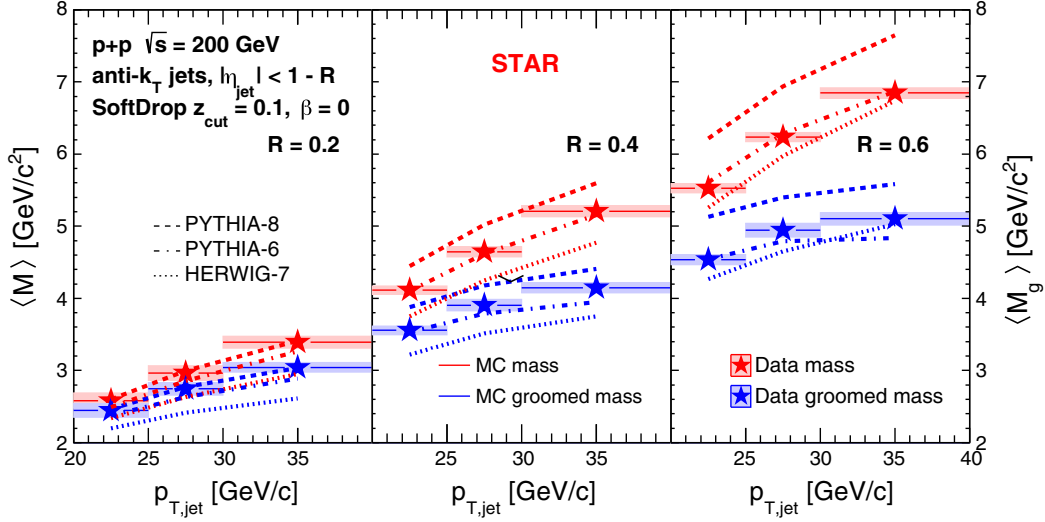
FIG. 6.   Mean jet mass of anti-k_T jets in pp collisions at $\sqrt{s} = 200$ GeV as a function of $p_{T,\text{jet}}$ (x axis) and jet radius, R (panels). The fully corrected data are shown as solid star markers with accompanying shaded band denoting systematic uncertainties on the mean. The mean jet mass, $\langle M \rangle$, is shown in red; mean groomed jet mass, $\langle M_g \rangle$, is shown in blue. Statistical uncertainties are smaller than the size of the markers. PYTHIA-6 (PERUGIA 2012 STAR Tune, dot-dashed line), PYTHIA-8 (MONASH 2013 Tune, dashed line), and HERWIG-7 (EE4C Tune, dotted line) are also presented, with red denoting $\langle M \rangle$ and blue denoting $\langle M_g \rangle$.

most R and $p_{T,\text{jet}}$ selections with the exception of $R = 0.2$ for PYTHIA-8, and $30 < p_{T,\text{jet}} < 40$ GeV/c, $R = 0.6$ for ungroomed HERWIG-7, where they do describe the data. The preference of HERWIG-7 and PYTHIA-8 for lower and higher $\langle M_g \rangle$, respectively, is consistent with the observed preference for narrower and wider splits, respectively, in Ref. [40].

The dependence of the mass on jet radius and $p_{T,\text{jet}}$ is made more apparent by Fig. 6 in which we plot the mean (groomed) mass for the same jet radius and $p_{T,\text{jet}}$ selections as above. Note the decrease in $\langle M \rangle$ from grooming due to removal of wide-angle radiation. Additionally, there is an increase in the difference between the groomed and ungroomed jet mass for higher-p_T jets, presumably due to the fact that high-p_T jets are more collimated, so more of the widest-angle radiation is captured in the jet cone before grooming, which the grooming procedure then reduces. We also observe that for small radius jets, the jet mass is relatively unaffected by grooming, as much of the wide-angle radiation will already have left the jet cone, while for large-radius jets grooming dramatically reduces $\langle M \rangle$. There is also a much stronger dependence of $\langle M_{(g)} \rangle$ on the jet radius than on the $p_{T,\text{jet}}$. The stronger dependence on the radius is expected from the generic form of the jet mass: $M^2 \sim p_{T,\text{jet}} \sum_{i \in J} p_{T,i} \Delta R_{iJ}^2$, where $p_{T,i}$ is the transverse momentum with respect to the jet axis and $\Delta R_{iJ}^2 = (\Delta \eta_{iJ})^2 + (\Delta \phi_{iJ})^2$ is the distance of the constituent i from the jet axis [29]. Lastly, we observe that in general, HERWIG-7 (PYTHIA-8) predicts a smaller (larger) $\langle M_{(g)} \rangle$ than data, while PYTHIA-6 is roughly consistent with data, as mentioned in the previous two paragraphs.

Finally, we compare the hadron-level fully corrected jet mass data to a PQCD calculation at next-to-leading order with NLL accuracy at the parton-level in Fig. 7. NP contributions are expected to be large for small R, small $p_{T,\text{jet}}$, and small M. Because of this large NP contribution to the calculation for $R = 0.2$ over the entire jet mass range, we show only $R = 0.4$ and $R = 0.6$ jets, and even for $R = 0.4$ jets, the lowest $p_{T,\text{jet}}$ range is dominated by these NP contributions. Similarly, theoretical calculations become unreliable at small M, so a simple linear extrapolation of the ungroomed jet mass to (0, 0) is done in Fig. 7 in order to provide a consistent overall normalization by which to compare the calculations and data. The uncertainty on the calculation is given by QCD scale variation by a factor of two about the chosen values, while keeping the relation between the collinear and soft scales and between the hard and jet scales fixed, as in Ref. [51]. Note also that the jet mass range for the comparison is $0 < M < 10$ GeV/c^2 so the normalization of the data in Figs. 5 and 7 is different.

Although NP effects are minimized at large R and $p_{T,\text{jet}}$, we observe a significant discrepancy in the jet mass between the calculation and data even for $R = 0.6$, $30 < p_{T,\text{jet}} < 40$ GeV/c ungroomed jets. Since N^{n}LO effects should be small at RHIC, this indicates not a failing of the fixed-order calculation, but rather the large effect of hadronization and other NP contributions to the jet mass, e.g., multiple-particle interactions, in the STAR kinematic regime. However, we do observe that, for larger radius jets, the groomed jet mass data and ungroomed jet mass calculation are comparable, indicating the suppression of NP effects with the SOFTDROP procedure. We notice as well that the calculation is comparable with PYTHIA-8 both for
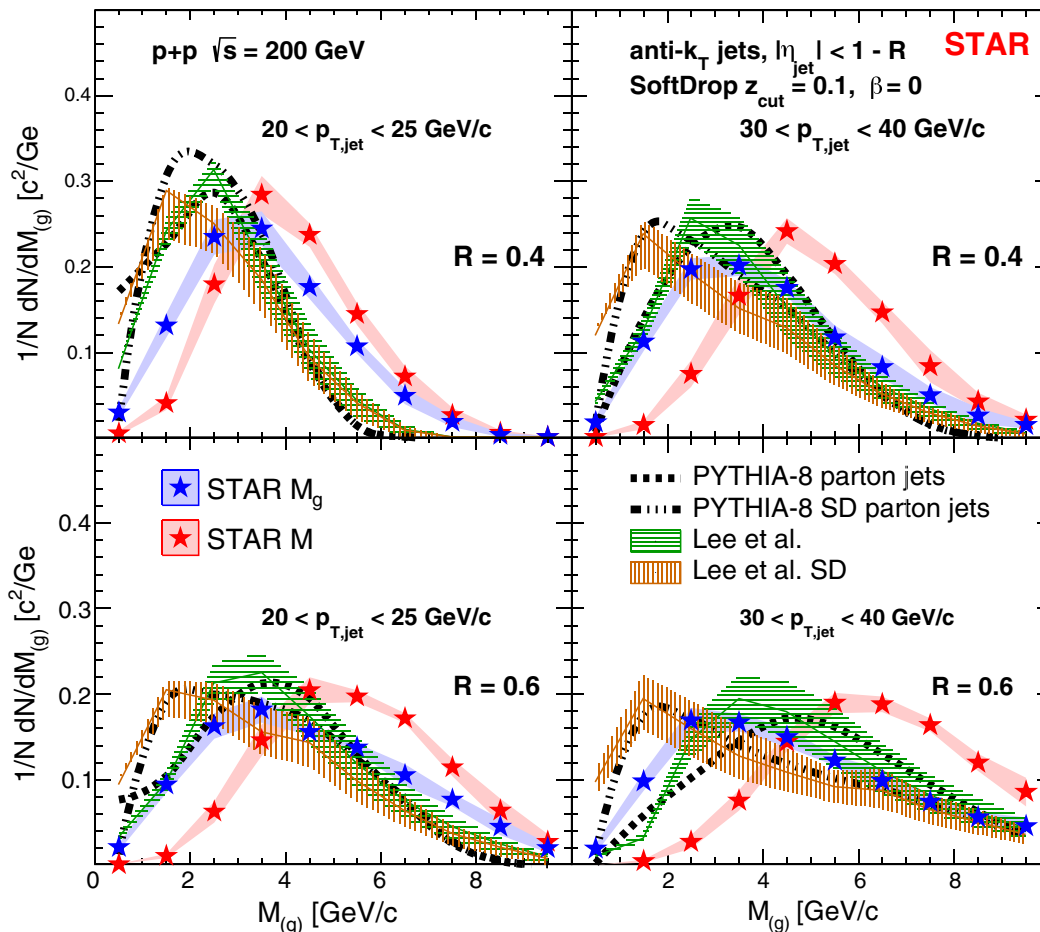
FIG. 7. Comparison between hadron-level fully corrected STAR data (star markers with shaded bands denoting systematic uncertainty) and a calculation at next-to-leading-log accuracy at parton level (shaded bands, which denote QCD scale variation uncertainty) as well as parton-level MC simulation, for M and M_g of anti-k_T jets in pp collisions at $\sqrt{s} = 200$ GeV for two $p_{\mathrm{T,jet}}$ selections (from left to right, $20 < p_{\mathrm{T,jet}} < 25$ GeV/c and $30 < p_{\mathrm{T,jet}} < 40$ GeV/c) and varying jet radii (from top to bottom, $R = 0.4, 0.6$). The ungroomed (groomed) jet mass data are in red (blue), while the ungroomed (groomed) jet mass calculation is in green (orange). Statistical uncertainties are smaller than the size of the markers. We additionally compare to groomed PYTHIA-8 parton-level (dot-dashed black line, denoted "SD" in the legend for SOFTDROP groomed jets) and ungroomed PYTHIA-8 parton-level (dashed black line). *N.B.* the calculation is dominated by NP effects below $M \approx 1$ GeV/c^2, so a linear extrapolation to zero was done from the lowest value above this NP regime.

groomed and ungroomed jets, which suggests that most of this large NP contribution is due to the hadronization of final-state particles. These results can be used to extract an NP shape function for a hadronization correction, and by extension they will allow for further refinement of theoretical quantities, such as the soft function, using the extracted R-dependent shape function [52].

VI. SUMMARY

This paper presents the first inclusive jet mass measurement in pp collisions at $\sqrt{s} = 200$ GeV at RHIC. Both the ungroomed and groomed jet mass are presented differentially in the jet radius and transverse momentum. We observe trends of increasing mean and width of the distributions with increased R due to the inclusion of more

wide-angle radiation. We observe the same trends for increasing $p_{\mathrm{T,jet}}$ as well due to the increased phase space for radiation. Both of these observations are consistent with PQCD. In addition, grooming is shown to shift the mass distribution to smaller values and reduce the position of the Sudakov peak, leaving the fully corrected groomed jet mass amenable to comparison with NLL calculations.

Although the fully corrected data is well-described by the RHIC-tuned leading-order MC event generator PYTHIA-6 PERUGIA 2012, it is not as well-described by LHC-tuned PYTHIA-8 MONASH 2013 and HERWIG-7 EE4C, providing crucial input for further RHIC tunes. This measurement will also serve as an important reference for future jet mass measurements in heavy-ion collisions at RHIC in which modification due to energy loss in the hot nuclear medium may be expected.

ACKNOWLEDGMENTS

[1] A. Ali and G. Kramer, Eur. Phys. J. H **36**, 245 (2011).

[2] Y. L. Dokshitzer, Sov. Phys. JETP **46**, 641 (1977).

[3] V. N. Gribov and L. N. Lipatov, Sov. J. Nucl. Phys. **15**, 438 (1972).

[4] G. Altarelli and G. Parisi, Nucl. Phys. **B126**, 298 (1977).

[5] M. Cacciari, G. P. Salam, and G. Soyez, J. High Energy Phys. 04 (2008) 063.

[6] P. A. Zyla *et al.* (Particle Data Group), Prog. Theor. Exp. Phys. **2020**, 083C01 (2020).

[7] A. M. Sirunyan *et al.* (CMS Collaboration), Eur. Phys. J. C **80**, 752 (2020).

[8] D. Gutierrez-Reyes, Y. Makris, V. Vaidya, I. Scimemi, and L. Zoppi, J. High Energy Phys. 08 (2019) 161.

[9] Y. Mehtar-Tani and K. Tywoniuk, Phys. Rev. D **98**, 051501 (2018).

[10] G. Aad *et al.* (ATLAS Collaboration), J. High Energy Phys. 05 (2012) 128.

[11] M. Aaboud *et al.* (ATLAS Collaboration), Phys. Rev. Lett. **121**, 092001 (2018).

[12] ATLAS Collaboration, Report No. ATLAS-CONF-2018-014, 2018.

[13] T. Aaltonen *et al.* (CDF Collaboration), Phys. Rev. D **85**, 091101 (2012).

[14] S. Chatrchyan *et al.* (CMS Collaboration), J. High Energy Phys. 05 (2013) 090.

[15] A. M. Sirunyan *et al.* (CMS Collaboration), Eur. Phys. J. C **77**, 467 (2017).

[16] A. M. Sirunyan *et al.* (CMS Collaboration), J. High Energy Phys. 10 (2018) 161.

[17] S. Acharya *et al.* (ALICE Collaboration), Phys. Lett. B **776**, 249 (2018).

[18] J. Adam *et al.* (STAR Collaboration), Phys. Rev. D **100**, 052005 (2019).

[19] T. Sjöstrand, S. Mrenna, and P. Z. Skands, J. High Energy Phys. 05 (2006) 026.

[20] T. Sjöstrand, S. Mrenna, and P. Z. Skands, Comput. Phys. Commun. **178**, 852 (2008).

[21] J. Bellm *et al.*, Eur. Phys. J. C **76**, 196 (2016).

[22] A. Moraes, C. Buttar, and I. Dawson, Eur. Phys. J. C **50**, 435 (2007).

[23] A. J. Larkoski, S. Marzani, and J. Thaler, Phys. Rev. D **91**, 111501 (2015).

[24] A. J. Larkoski, S. Marzani, G. Soyez, and J. Thaler, J. High Energy Phys. 05 (2014) 146.

[25] D. Anderle, M. Dasgupta, B. K. El-Menoufi, J. Helliwell, and M. Guzzi, Eur. Phys. J. C **80**, 827 (2020).

[26] M. Dasgupta, A. Fregoso, S. Marzani, and G. P. Salam, J. High Energy Phys. 09 (2013) 029.

[27] A. Majumder and J. Putschke, Phys. Rev. C **93**, 054909 (2016).

[28] M. Balsiger, T. Becher, and D. Y. Shao, J. High Energy Phys. 04 (2019) 020.

[29] Z.-B. Kang, K. Lee, X. Liu, and F. Ringer, Phys. Lett. B **793**, 41 (2019).

[30] J. Chay and C. Kim, J. Korean Phys. Soc. **74**, 439 (2019).

[31] Z.-B. Kang, K. Lee, X. Liu, and F. Ringer, J. High Energy Phys. 10 (2018) 137.

[32] Z.-B. Kang, K. Lee, and F. Ringer, J. High Energy Phys. 04 (2018) 110.

[33] S. Marzani, L. Schunk, and G. Soyez, Eur. Phys. J. C **78**, 96 (2018).

[34] A. Idilbi and C. Kim, J. Korean Phys. Soc. **73**, 1230 (2018).

[35] Z. L. Liu, C. S. Li, J. Wang, and Y. Wang, J. High Energy Phys. 04 (2015) 005.

[36] M. Cacciari, G. P. Salam, and G. Soyez, Eur. Phys. J. C **72**, 1896 (2012).

[37] M. Anderson *et al.*, Nucl. Instrum. Methods Phys. Res., Sect. A **499**, 659 (2003).

[38] M. Beddo *et al.* (STAR Collaboration), Nucl. Instrum. Methods Phys. Res., Sect. A **499**, 725 (2003).

[39] L. Adamczyk *et al.* (STAR Collaboration), Phys. Rev. Lett. **115**, 092002 (2015).

[40] J. Adam *et al.* (STAR Collaboration), Phys. Lett. B **811**, 135846 (2020).

[41] Y. L. Dokshitzer, G. Leder, S. Moretti, and B. Webber, J. High Energy Phys. 08 (1997) 001.

[42] M. Wobisch and T. Wengler, in *Workshop on Monte Carlo Generators for HERA Physics (Plenary Starting Meeting)* (1998), p. 270 [arXiv:hep-ph/9907280].

[43] G. D'Agostini, arXiv:1010.0632.

[44] T. Adye, in *PHYSTAT 2011* (CERN, Geneva, 2011), p. 313.

[45] J. Pumplin, D. Stump, J. Huston, H. Lai, P. M. Nadolsky, and W. Tung, J. High Energy Phys. 07 (2002) 012.

[46] R. Brun, F. Bruyant, F. Carminati, S. Giani, M. Maire, A. McPherson, G. Patrick, and L. Urban (1994).

[47] J. Gallicchio and M. D. Schwartz, J. High Energy Phys. 04 (2013) 090.

[48] P. Z. Skands, Phys. Rev. D **82**, 074018 (2010).

[49] P. Skands, S. Carrazza, and J. Rojo, Eur. Phys. J. C **74**, 3024 (2014).

[50] M. H. Seymour and A. Siodmok, J. High Energy Phys. 10 (2013) 113.

[51] E.-C. Aschenauer, K. Lee, B. S. Page, and F. Ringer, Phys. Rev. D **101**, 054028 (2020).

[52] I. W. Stewart, F. J. Tackmann, and W. J. Waalewijn, Phys. Rev. Lett. **114**, 092001 (2015).

Correction: Some affiliations we set incorrectly during the production process and have been fixed.